Available online at www.sciencedirect.com
SCIENCE DIRECT®
Journal of Sound and Vibration 268 (2003) 637–656
JOURNAL OF SOUND AND VIBRATION
www.elsevier.com/locate/jsvi

Free vibration of skew Mindlin plates by *p*-version of F.E.M.

K.S. Woo[a,*], C.H. Hong[a,1,2], P.K. Basu[a], C.G. Seo[b]

[a] *Department of Civil & Environmental Engineering, Vanderbilt University, TN 37235, USA*
[b] *Department of Civil Engineering, KAIST, Daejon 305-701, South Korea*

Received 14 January 2002; accepted 21 November 2002

Abstract

Accurate natural frequencies and mode shapes of skew plates with and without cutouts are determined by *p*-version finite element method using integrals of Legendre polynomials for $p = 1$–14. The hierarchical plate element is formulated based on Mindlin's plate theory including rotatory inertia effects and based on a skew co-ordinate system. Non-dimensional frequency parameter and mode shapes are presented for a range of skew angle (β), aspect ratio (a/b), thickness–width ratio (h/b), cutout dimensions and different boundary conditions. The results were verified by comparison with those available in the open literature.

1. Introduction

Skew plates are characterized by the presence of strong moment singularity at the supported obtuse corners. No exact solution is suitable for the problem but the analytical approximate solution by Morley [1] is considered to be accurate enough. This problem attracted much attention in 1970s with reference to fatigue life prediction of aircrafts with swept wings, which have an obtuse corner at its junction with the fuselage. Although a number of researchers have studied the free vibration of clamped, simply supported and free edged skew plates, there is still the need to obtain reliable results with reasonable effort. A review of previous work is available in a monograph and in subsequent articles by Leissa [2,3]. Various methods have been attempted to analyze the free vibration of simply supported skew plates, such as the boundary collocation technique by Conway and Farnham [4], the Ritz method by Nair and Purvasula [5], and the edge

*Corresponding author: Department of Civil Engineering, Yeungnam University, Gyeongsan 712-749, South Korea. E-mail address: kswoo@yu.ac.kr.
[1] Visiting scholar of Vanderbilt University in 2001.
[2] Department of Civil Engineering of Tamna University, Seoguipo 697-340, South Korea.

0022-460X/03/$ - see front matter
doi:10.1016/S0022-460X(02)01536-5

function method by Tai and Nash [6]. Chopra and Durvasula [7] used Lagrange equation based on the normal displacement of plate defined as a double Fourier sine series in the skew co-ordinate to obtain the approximate frequencies for tapered skew plates. Using the analogy between membrane and flexural mode of simply supported polygonal plates, Sakata [8] derived the approximate formula for the fundamental frequency of simply supported skew plates. Nagaya [9] put forward the analytical solution, which includes the ordinary Bessel function with an integer order and Fourier expansion for different boundary conditions. Apart from these analytical treatments, further developments in the vibration problem of simply supported skew plates have been minimal [3]. Some accurate results for simply supported rhombic and parallelogram plates have, however, been presented recently by Gorman [10] using the superposition method. Besides this, some experimental vibration data have surfaced in recent years for simply supported skew plates due to Rao et al. [11].

Using finite element modelling, Raju and Hinton [12] made significant contributions in vibration analysis plates including rotatory inertia effects for rhombic plates with various boundary conditions. They used nine-noded Lagrangian quadrilateral isoparametric plate elements based on Mindlin's theory. McGee [13,14] determined the natural frequencies of skewed and twisted cantilevered thick plates by the Ritz method. Because of merits of hierarchical element, Bardell [15] applied the Legendre orthogonal polynomials to obtain the natural frequencies and modes of a flat, rectangular plate. On the other hand, Beslin and Nicolas [16] proposed a new hierarchical function set built from trigonometric functions instead of polynomials. However, the studies using these hierarchical plate elements were limited to analysis of rectangular plates. The hierarchical concept showed fast convergence and higher accuracy compared with the conventional *h*-version of the finite element method (*h*-FEM). Basu et al. [17] were the first to investigate stress singularities at the obtuse corner using four fifth order hierarchical Legendre elements to model a quadrant of a simply supported 60° plate under uniformly distributed load. Huang et al. [18] investigated the stress singularities in the obtuse corners of rhombic plates based on the Ritz method using a hybrid set consisting two types of displacement function such as algebraic polynomials and the corner function accounting for corner singularities. Butalia et al. [19] used the Heterosis element for bending of skew rhombic plates. Based on the Ritz method along with Mindlin's plate theory, Liew et al. [20–23] obtained highly accurate results by using the hierarchical Legendre polynomials.

The *p*-version of the finite element method (*p*-FEM) is well recognized as a powerful numerical modelling tool, which shows the merits of hierarchical nature, well-conditioned system of equations, fast convergence rate, and simple modelling. The aim of this paper is three-fold. Firstly, the hierarchical set of integrals of Legendre polynomials is generated ranging from $p = 1$ to 14. Secondly, the energy functional is derived from the skew co-ordinate system with proper co-ordinate transformations that also include the rotatory inertia effects. Finally, the accuracy and the convergence characteristics of non-dimensional frequency parameters and mode shapes are investigated by analyzing skew Mindlin plates with or without cutout for a range of skew angles (β), aspect ratios (a/b), thickness-to-width ratios (h/b), and various boundary conditions. The present *p*-version solutions have been compared with the published results and the *h*-version finite element results by using SAP2000 commercial software.

2. Formulation of skew Mindlin plates

2.1. Energy functional for skew Mindlin plates

From Fig. 1, the geometric and material configurations of a flat, isotropic, skew plate are defined by uniform thickness h, length a, oblique width b, skew angle β, Young's modulus E, shear modulus G, the Poisson ratio v, and shear correction factor κ. The strain and kinetic energies can be expressed in tensor form as

$$U = \frac{1}{2}\int_V \boldsymbol{\tau}_{ij}\boldsymbol{\varepsilon}_{ij}\,\mathrm{d}V, \tag{1}$$

$$T = \frac{1}{2}\int_V \boldsymbol{\rho}\dot{u}_i\dot{u}_j,\,\mathrm{d}V. \tag{2}$$

Using appropriate constitutive relationships, Eq. (1) can also be written as

$$U = \frac{1}{2}\int \boldsymbol{\varepsilon}_{ij}^T[\mathrm{D}]\varepsilon_{ij}\,\mathrm{d}V. \tag{3}$$

In this equation, the strain tensor is denoted by $\varepsilon_{ij}^{\mathrm{T}} = \lfloor \varepsilon_{xx}\varepsilon_{yy}\gamma_{xy}\gamma_{xz}\gamma_{yz} \rfloor$, $\boldsymbol{V}$ is the volume of the plate, and [**D**] is the constitutive matrix. With u_1, u_2, u_3 as the displacement components in x, y and z directions, and $\theta_x(x,y,t)$, $\theta_y(x,y,t)$ as the rotations along x and y directions, by Green's definition of strains, it follows

$$\varepsilon_{ij} = \begin{Bmatrix} \varepsilon_{xx} \\ \varepsilon_{yy} \\ \gamma_{xy} \\ \gamma_{xz} \\ \gamma_{yz} \end{Bmatrix} = \begin{Bmatrix} \frac{\partial u_1}{\partial x} \\ \frac{\partial u_2}{\partial y} \\ \frac{\partial u_1}{\partial y} + \frac{\partial u_2}{\partial x} \\ \frac{\partial u_1}{\partial z} + \frac{\partial u_3}{\partial x} \\ \frac{\partial u_2}{\partial z} + \frac{\partial u_3}{\partial y} \end{Bmatrix} = \begin{Bmatrix} z\frac{\partial \theta_x}{\partial x} \\ z\frac{\partial \theta_y}{\partial y} \\ z(\frac{\partial \theta_x}{\partial y} + \frac{\partial \theta_y}{\partial x}) \\ \theta_x + \frac{\partial w}{\partial x} \\ \theta_y + \frac{\partial w}{\partial y} \end{Bmatrix}. \tag{4}$$

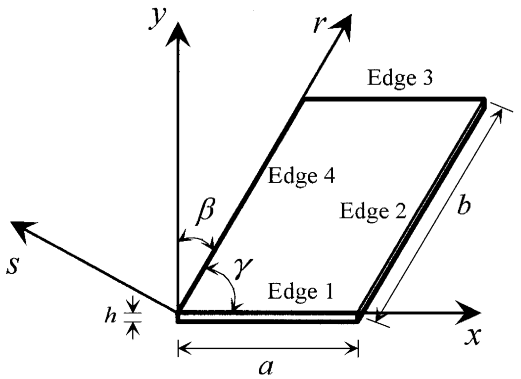

Fig. 1. Geometry and co-ordinate system of skew plates.

The constitutive matrix is given by

$$[D] = \begin{bmatrix} \frac{E}{(1-\nu^2)} & \frac{\nu E}{(1-\nu^2)} & 0 & 0 & 0 \\ \frac{\nu E}{(1-\nu^2)} & \frac{E}{(1-\nu^2)} & 0 & 0 & 0 \\ 0 & 0 & G & 0 & 0 \\ 0 & 0 & 0 & \kappa G & 0 \\ 0 & 0 & 0 & 0 & \kappa G \end{bmatrix}, \qquad G = \frac{E}{2(1+\nu)}, \tag{5}$$

in which the shear factor, $\kappa = 0.83333$ for $\nu = 0.3$.

Thus, the strain and kinetic energies in the rectangular co-ordinate system can be expressed in terms of w, θ_x and θ_y as

$$U = \frac{1}{2}\int\int_A \left\{ \left[D^2 \left(\frac{\partial \theta_x}{\partial x} + \frac{\partial \theta_y}{\partial y} \right) - 2(1-\nu) \left(\frac{\partial \theta_x}{\partial x}\frac{\partial \theta_y}{\partial y} - \frac{1}{4}\left(\frac{\partial \theta_x}{\partial y} + \frac{\partial \theta_y}{\partial x} \right)^2 \right) \right] + k^2 Gh \left[\left(\theta_x + \frac{\partial w}{\partial x} \right)^2 + \left(\theta + \frac{\partial w}{\partial y} \right)^2 \right] \right\}, \tag{6}$$

$$T = \frac{1}{2}\rho h \omega^2 \int\int_A \left\{ w^2 + \frac{h^2}{12}\left(\theta_x^2 + \theta_y^2 \right) \right\} \mathrm{d}A, \tag{7}$$

where ρ is the mass density per unit volume, and ω is the circular frequency. Eq. (7) includes the rotatory inertia effects that become significant in the lower flexural modes for thicker plates.

2.2. Oblique boundary transformation

As shown in Fig. 1, both the edges of a skew plate may not be parallel to global axes x and y. So, it is difficult to define the boundary conditions in terms of the global displacements w, θ_x and θ_y. To specify the boundary conditions at such edges, the local edge displacements w, θ_r and θ_s shown in Fig. 2 can be used. Here, θ_r and θ_s represent the average rotations of the normal to the

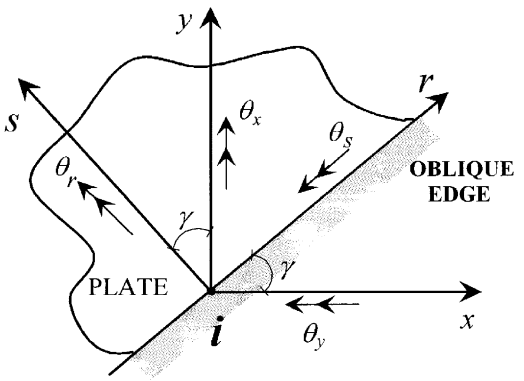

Fig. 2. Global and local skew co-ordinate system for oblique boundary transformation.

reference plane, tangential and normal to the oblique edge. Before enforcement of the boundary conditions at such edges, it is necessary to transform the element matrices corresponding to global axes (x, y) along which the boundary conditions are specified. Considering θ_x, θ_y, θ_r and θ_s as vectors shown in Fig. 2, where γ is denoted by $\gamma = 90-\beta$, the displacement transformation for a node "*i*"on the oblique boundary is given by

$$\begin{Bmatrix} w \\ \theta_x \\ \theta_y \end{Bmatrix} = \begin{bmatrix} 1 & 0 & 0 \\ 0 & \cos\gamma & -\sin\gamma \\ 0 & \sin\gamma & \cos\gamma \end{bmatrix} \begin{Bmatrix} w \\ \theta_r \\ \theta_s \end{Bmatrix}. \tag{8}$$

This transformation relationship will be expressed as

$$\mathbf{u}_i = \mathbf{T}_{ij} \cdot \bar{\mathbf{u}}_j, \tag{9}$$

where $\mathbf{u}_i$ and $\bar{\mathbf{u}}_j$ are the generalized displacement vectors in the global and local edge co-ordinate systems. The above matrix is valid only for three degrees of freedom per node. For nodes, which are not located on the oblique boundary, it becomes an unit matrix. Thus, for an n-noded boundary element, the element transformation matrix can be expressed as

$$[T] = \begin{bmatrix} T_1 & & & & & & \\ & T_2 & & & & & \\ & & \ddots & & & & \\ & & & T_i & & & \\ & & & & \ddots & & \\ & & & & & T_n & \end{bmatrix}. \tag{10}$$

2.3. Eigenvalue problem for skew plates

The governing equation of motion may be derived from the Hamilton's principle, which requires the functional to satisfy the condition

$$\delta \int_{t^i}^{t^f} \Pi = \delta \int_{t^i}^{t^f} (\boldsymbol{U} - \boldsymbol{T})\, \mathrm{d}t = \delta \left[\frac{1}{2} \int_{t_i}^{t_f} \int_V \tau_{ij}\varepsilon_{ij}\, \mathrm{d}V\, \mathrm{d}t - \int_{t_i}^{t_f} \int_V \rho \ddot{u}_i \dot{u}_j\, \mathrm{d}V\, \mathrm{d}t \right] = 0, \tag{11}$$

where δ is the variational operator and it moves from the configuration "*i*" at time t_i to the configuration "*f*" at time t_f. The displacement field over an element can be defined by $\boldsymbol{u}=\boldsymbol{\Psi}\boldsymbol{u}^e$ where $\boldsymbol{u}^e$ is the vector of nodal displacements and nodeless coefficients, and $\boldsymbol{\Psi}$ is the interpolation function in terms of integrals of Legendre polynomials. After differentiating Eq. (11) with respect to time, the final energy functional expressed in matrix form can be obtained after substituting the strain–displacement and constitutive relationships.

$$\Pi_e = \frac{1}{2} \int_V [u^e]^{\mathrm{T}} [T]^{\mathrm{T}} [B]^{\mathrm{T}} DBTu^e\, \mathrm{d}V - \frac{1}{2} \int_V \frac{\mathrm{d}[u^e]^{\mathrm{T}}}{\mathrm{d}t} [T]^{\mathrm{T}} [\Psi]^{\mathrm{T}} \rho \Psi T \frac{\mathrm{d}u^e}{\mathrm{d}t}\, \mathrm{d}V. \tag{12}$$

The minimization of energy functional with respect to the nodal displacement $\boldsymbol{u}^e$ for an element results in

$$\frac{\partial \Pi_e}{\partial u^e} = \int_V ([T]^{\mathrm{T}}[B]^{\mathrm{T}} DBT) u^e \, \mathrm{d}V - \int_V \left(\frac{\mathrm{d}[u^e]^{\mathrm{T}}}{\mathrm{d}t}\right)([T]^{\mathrm{T}}[\Psi]^{\mathrm{T}} \rho \Psi T)\left(\frac{\mathrm{d}u^e}{\mathrm{d}t}\right) \mathrm{d}V. \tag{13}$$

The element stiffness and the mass matrices are then arrived at after mapping into the standard (ξ,η) co-ordinate system as

$$\mathbf{K}_{ij}^e = \int_{V_e} [T]^{\mathrm{T}}[B]^{\mathrm{T}} DBT \, \mathrm{d}V = \int \int_{A_e} [T]^{\mathrm{T}}[B]^{\mathrm{T}} DBT \, h \det J \, \mathrm{d}\xi \, \mathrm{d}\eta, \tag{14}$$

$$\mathbf{M}_{ij}^e = \int_{V_e} [T]^{\mathrm{T}}[\Psi]^{\mathrm{T}} \rho \Psi T \, \mathrm{d}V = I_0 \int \int_{A_e} [T]^{\mathrm{T}}[\Psi]^{\mathrm{T}} \Psi \, T \det J \, \mathrm{d}\xi \, \mathrm{d}\eta, \tag{15}$$

where $\det J \, \mathrm{d}\xi \, \mathrm{d}\eta = \mathrm{d}x \, \mathrm{d}y$, $I_o = \rho h$, Also, $[\Psi]$ is the matrix of shape functions given by

$$[\boldsymbol{\Psi}_i]_{(3\times(3*n))} = \begin{bmatrix} \Psi_1 & 0 & 0 & \Psi_2 & 0 & 0 & \cdots & \Psi_i & 0 & 0 & \cdots & \Psi_n & 0 & 0 \\ 0 & \Psi_1 & 0 & 0 & \Psi_2 & 0 & \cdots & 0 & \Psi_i & 0 & \cdots & 0 & \Psi_n & 0 \\ 0 & 0 & \Psi_1 & 0 & 0 & \Psi_2 & \cdots & 0 & 0 & \Psi_i & \cdots & 0 & 0 & \Psi_n \end{bmatrix}. \tag{16}$$

The mass matrix in Eq. (15) neglects the rotatory inertia effects of Mindlin plate. So the inertia term $I_2 = 1/(12\rho h^2)$ should be introduced into Eq. (13) to get the eigen equation for a Mindlin plate. It may be noted that this mass matrix is consistent but for a homogeneous system can be approximated as a diagonal one, as shown in Eq. (17)

$$\left[\begin{bmatrix} K_{11}^e & K_{12}^e & K_{13}^e \\ & K_{22}^e & K_{23}^e \\ sym & & K_{33}^e \end{bmatrix} - \omega^2 \begin{bmatrix} I_o M_{11}^e & 0 & 0 \\ & I_2 M_{22}^e & 0 \\ sym & & I_2 M_{33}^e \end{bmatrix}\right] \begin{Bmatrix} w^e \\ \theta_x^e \\ \theta_y^e \end{Bmatrix} = 0 \tag{17}$$

which can be expressed in compact form as

$$[\mathbf{K}]_p - \boldsymbol{\lambda}_i [\mathbf{M}]_p = 0, \tag{18}$$

where p is degree of square matrix, λ_i is the eigenvalue with $\lambda_i = \{\lambda_1 \cdots \lambda_k \cdots \lambda_p\}^{\mathrm{T}}$, Δ_i is the eigenvector with $\Delta_i = \{\Delta_1 \cdots \Delta_k \cdots \Delta_p\}^{\mathrm{T}}$ that is corresponding to λ_i. Also, the eigenvector must satisfy the orthogonality conditions like $\boldsymbol{\Delta}_i^{\mathrm{T}} \mathbf{K} \boldsymbol{\Delta}_i = \lambda_i$ and $\boldsymbol{\Delta}_i^{\mathrm{T}} \mathbf{M} \boldsymbol{\Delta}_i = \mathbf{I}$. Standard Houserholder QR iteration technique is adopted to solve the eigen equation.

3. Hierarchical polynomials set

It is preferable to use shape functions that give a strongly diagonal element stiffness matrix. In this paper, a hierarchical system of shape functions on the basis of integrals of Legendre polynomials is used. The first set of 14 shape functions are given in Table 1.

Table 1
The first set of 14 hierarchical shape functions

p-Level	$\boldsymbol{F}(\xi)$; $-1 \leqslant \xi \leqslant 1$
1	$\frac{1}{2}(\xi-1)$
2	$\frac{3}{2\sqrt{6}}(\xi^2-1)$
3	$\frac{5}{2\sqrt{1}}(\xi^3-\xi)$
4	$\frac{1}{8\sqrt{14}}(35\xi^4-42\xi^2+7)$
5	$\frac{1}{8\sqrt{18}}(63\xi^5-90\xi^3+27\xi)$
6	$\frac{1}{16\sqrt{22}}(231\xi^6-385\xi^4+165\xi^2-11)$
7	$\frac{1}{16\sqrt{26}}(429\xi^7-819\xi^5+455\xi^3-65\xi)$
8	$\frac{1}{128\sqrt{30}}(6435\xi^8-13860\xi^6+9450\xi^4-2100\xi^2+75)$
9	$\frac{1}{128\sqrt{34}}(12155\xi^9-29172\xi^7+23562\xi^5-7140\xi^3+595\xi)$
10	$\frac{1}{256\sqrt{38}}(46189\xi^{10}-122265\xi^8+114114\xi^6-43890\xi^4+5985\xi^2-133)$
11	$\frac{1}{256\sqrt{42}}(88179\xi^{11}-255255\xi^9+270270\xi^7-126126\xi^5+24255\xi^3-1323\xi)$
12	$\frac{1}{512\sqrt{46}}(338019\xi^{12}-1062347\xi^{10}+1258042\xi^8-690690\xi^6+172672\xi^4-15939\xi^2+242)$
13	$\frac{1}{512\sqrt{50}}(650038\xi^{13}-2204475\xi^{11}+2886812\xi^9-1823250\xi^7+563062\xi^5-75075\xi^3+2888\xi)$
14	$\frac{1}{1024\sqrt{54}}(2507288\xi^{14}-9126526\xi^{12}+13094582\xi^{10}-9353272\xi^8+3445942\xi^6-608108\xi^4+40540\xi^2-446)$

4. Numerical results

4.1. Skew plates without cut-out

The six different edge conditions considered are shown in Table 2. The symbols S, F, and C indicate simply supported, free and clamped, respectively. The Poisson ratio (v) is fixed as 0.3. In the parametric study, three geometric parameters are varied, namely, thickness ratio (h/b), aspect ratio(a/b) and skew angle (β).

In Tables 3–6 are given the first six modal non-dimensional frequencies, $\lambda[=(\omega b^2/\pi^2)\sqrt{\rho h/D}]$ where ω is the circular frequency, ρ is the mass density per unit volume, and $D = Eh^3/12(1-v^2)$. The thickness ratio (h/b) is taken to be 0.001 for thin plates and 0.2 for thick plates. The validity of the "thin" plate results is confirmed by existing solutions computed by Raju and Hinton [12],

Table 2
Definition of different edge conditions

Case	Edge 1	Edge 2	Edge 3	Edge 4
1	S	S	S	S
2	S	F	S	F
3	S	C	S	C
4	C	C	C	C
5	C	F	C	F
6	C	F	F	F

Table 3
Frequency parameters $\lambda = (\omega b^2/\pi^2)\sqrt{\rho h/D}$ of skew plates for Case 1 edge condition (a/b=1.0, v=0.3, β=15°)

h/b	Frequency mode	Non-dimensional frequency λ			
		p-FEM	Liew [23]	Raju [12]	Huang [18]
0.001	1	2.1149	2.1147	2.117	2.1144
	2	4.8841	4.8842	4.903	4.8842
	3	5.6872	5.6856	5.712	5.6848
	4	8.0090	8.0090	8.069	8.0087
	5	10.5377	10.5372	10.76	10.5374
	6	11.0277	11.0337	—	—
0.2	1	1.80256	1.8560	1.860	—
	2	3.72284	3.7856	3.803	—
	3	4.21581	4.2763	4.300	—
	4	5.43977	5.5784	5.617	—
	5	6.78359	6.8385	6.947	—
	6	7.01248	7.0702	—	—

Table 4
Frequency parameters $\lambda = (\omega b^2/\pi^2)\sqrt{\rho h/D}$ of skew plates for Case 1 edge condition (a/b=1.0, v=0.3, β=45°)

h/b	Frequency mode	Non-dimensional frequency λ			
		p-FEM	Liew [23]	Raju [12]	Huang [18]
0.001	1	3.5871	3.5800	3.6648	3.5208
	2	6.7168	6.7153	6.7632	6.7153
	3	10.1984	10.1756	10.1979	10.1574
	4	11.0746	10.9754	11.2467	10.8454
	5	14.3240	14.2662	14.8334	14.2660
	6	17.1028	17.0518	—	—
0.2	1	2.87991	2.9129	2.968	—
	2	4.79547	4.8736	4.909	—
	3	6.50515	6.6622	6.767	—
	4	6.98927	7.0148	7.129	—
	5	8.36149	8.4831	8.698	—
	6	9.50514	9.5878	—	—

Table 5
Frequency parameters $\lambda = (\omega b^2/\pi^2)\sqrt{\rho h/D}$ of skew plates for Case 4 edge condition ($a/b = 1.0$, $v = 0.3$, $\beta = 15^\circ$)

h/b	Frequency	Non-dimensional frequency λ			
	mode	p-FEM	Liew [23]	Raju [12]	Huang [18]
0.001	1	3.8679	3.8691	3.872	3.8692
	2	7.3865	7.3858	7.421	7.3859
	3	8.3757	8.3708	8.410	8.3710
	4	11.1094	11.1005	11.180	11.1009
	5	14.1151	14.0806	14.370	14.0810
	6	14.7423	14.7064	—	14.7070
0.2	1	2.7882	2.8058	2.815	—
	2	4.6108	4.6298	4.655	—
	3	5.0869	5.0963	5.125	—
	4	6.2708	6.3070	6.346	—
	5	7.3881	7.4052	7.493	—
	6	7.7050	7.7179	—	—

Table 6
Frequency parameters $\lambda = (\omega b^2/\pi^2)\sqrt{\rho h/D}$ of skew plates for Case 4 edge condition ($a/b = 1.0$, $v = 0.3$, $\beta = 45^\circ$)

h/b	Frequency	Non-dimensional Frequency λ			
	Mode	p-FEM	Liew [23]	Raju [12]	Huang [18]
0.001	1	6.65751	6.6519	6.665	6.6510
	2	10.82592	10.7898	10.9	10.7902
	3	15.22984	15.0276	15.36	15.0271
	4	16.1277	15.9342	16.09	15.9313
	5	20.5724	19.9395	20.77	19.9373
	6	23.67016	23.2526	—	23.2523
0.2	1	4.1622	4.1590	4.178	—
	2	5.9043	5.9021	5.947	—
	3	7.4729	7.5422	7.628	—
	4	7.8007	7.7907	7.849	—
	5	9.2237	9.2159	9.374	—
	6	10.1056	10.0921	—	—

Huang et al. [18] and Liew et al. [23], while the results for "thick" plates compare well with those obtained by Raju and Hinton [12], Liew et al. [23] who consider the effects of shear deformation and rotatory inertia. In these tables, two boundary conditions of SSSS (Case 1) and CCCC (Case 4) are considered.

In Tables 3 and 4, the results for Case 1 edge conditions and skew angle $\beta = 15^\circ$ and 45° are presented; whereas, in Tables 5 and 6, the results are for Case 4 edge conditions and skew angle $\beta = 15^\circ$ and 45°. The p-version solutions obtained with a one-element model and p-level = 7 are in excellent agreement with the results in literatures. In the case of both thin and thick plates, the relative error in λ is found to be less than 1.0%.

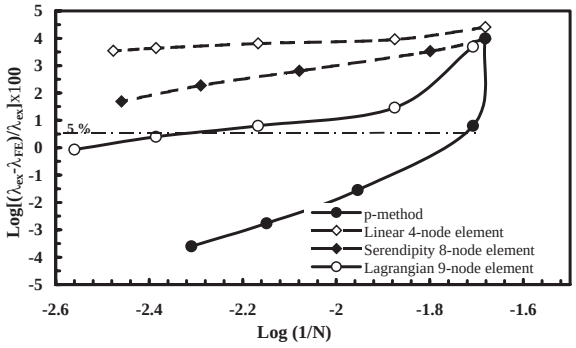

Fig. 3. Relative error λ for different finite element models.

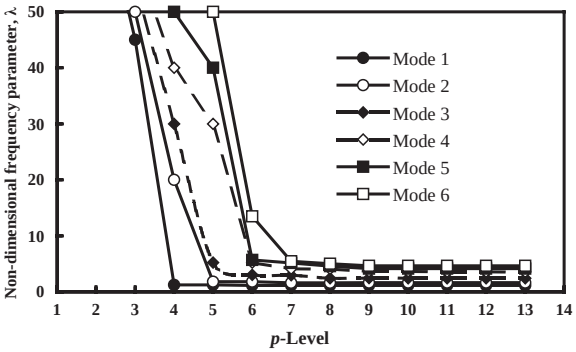

Fig. 4. Convergence characteristics of λ for single-element p-version model. ($a/b = 2.5$, $h/b = 0.001$, $\beta = 15^\circ$).

The p-version of the finite element method enables the accuracy of solution to be improved by adding hierarchical modes of high order without the need to change geometry of the mesh size. Accordingly, a p-version convergence study was undertaken and compared with the h-version. Fig. 3 shows the results of the study in the form of a log–log plot of relative error in non-dimensional frequency parameter versus the inverse of degree of freedoms.

It is evident from the figure that the convergence rate of p-version for the first mode is much faster than that for other h-version methods. For a solution with 5% of relative error, Log$(1/N)$ is approximately $-1.72(N = 53)$ for p-version model, and -2.32 $(N = 209)$ for Lagrangian nine-node element. It signifies that to achieve 5% of relative accuracy, the required number of degrees of freedom by h-version is four times that for p-version. Although uniform and monotonic convergence with increasing hierarchical shape functions is guaranteed, it is important to realize that the rate of convergence will, in general, be influenced by both the skew angle and the boundary conditions from the convergence tests. In this paper, only one convergence test result has been presented for Case 1 edge condition as an example where the aspect ratio a/b, thickness ratio h/b and skew angle β were fixed as 2.5, 0.001 and 15°, respectively. For this test, three different p-version finite element models are considered, such as a single-element model with p-level = 3–13, a four-element model with p-level = 2–10, and a nine-element model with p-level = 2–7. The results are presented in Figs. 4–6, which show the effect of non-dimensional

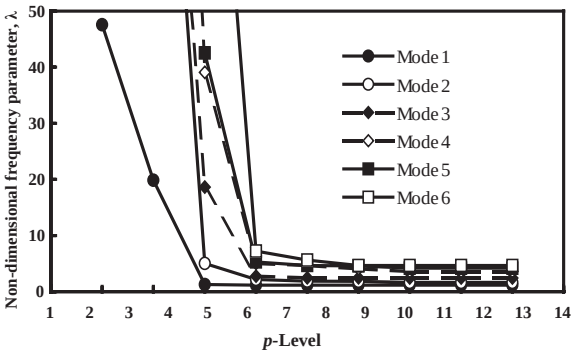

Fig. 5. Convergence characteristics of λ for four-element p-version model. ($a/b=2.5$, $h/b=0.001$, $\beta=15^\circ$).

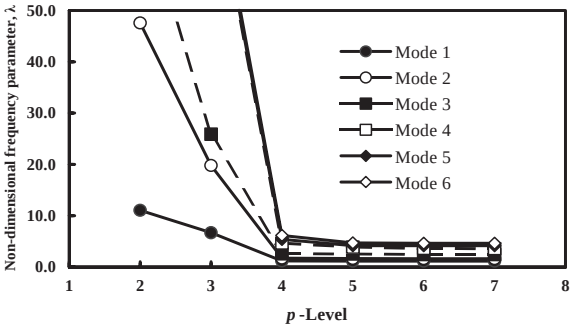

Fig. 6. Convergence characteristics of λ for nine-element p-version model. ($a/b=2.5$, $h/b=0.001$, $\beta=15^\circ$).

frequencies for the first six modes as the p-level is increased. As p-level is increased, λ tends to converge to the exact solution at a steep angle. It is evident from Fig. 4, that in case of single-element model, the solution tends to converge at p-level = 7. From Fig. 5 it is clear that in the case of four-element model, the solution tends to converge at p-level = 5. Finally, it can be seen from Fig. 6 that in the case of nine-element model, the solution tends to converge at p-level = 4.

To study the effect of boundary conditions, Tables 7 and 8 are also examined. It can be seen that the frequency parameters increase with higher constraint (from simply supported to fully clamped) at the four edges. This is due to the increased flexural stiffness when more edge constraints are introduced. It may be also noted that a higher frequency response has been observed as an increase in skew angle enhances the flexural stiffness of plates. Furthermore, the effect of aspect ratios a/b on the vibratory response has been studied. As shown in Fig. 7, the frequency parameters decrease as a/b ratios are increased.

To validate the accuracy of p-version finite element model, the non-dimensional fundamental frequency λ_1 of thin skew plates with various edge conditions has been compared to those obtained by Liew et al. [23], Raju and Hinton [12] where six edge conditions are considered. Table 9 also includes frequencies for plates where the geometric boundary condition for any simply supported edge has been expressed alternatively as $w=0$ in the paper of Raju and Hinton [12]. In this study, however, $w=\theta_t=0$ is used for simply supported edge by using exact oblique boundary transformation between global and local skew co-ordinate system shown in Fig. 2.

Table 7
Frequency parameters $\lambda = (\omega b^2/\pi^2)\sqrt{\rho h/D}$ of skew thin plates with various edge conditions ($a/b = 1.0$, $v = 0.3$, $h/b = 0.001$)

Edge condition	Mode number	Skew angle β				
		0°	15°	30°	45°	60°
Case 1	1	1.9999	2.1149	2.5380	3.5871	6.9160
	2	4.9999	4.8841	5.3333	6.7168	10.662
	3	5.0000	5.6872	7.3019	10.198	15.221
	4	7.9999	8.0090	8.5009	11.075	20.263
	5	9.9999	10.538	12.451	14.324	22.070
Case 2	1	0.9759	1.0333	1.2314	1.6696	2.6195
	2	1.6348	1.6696	1.7951	2.0807	2.7684
	3	3.7210	3.6440	3.6489	4.0146	5.4625
	4	3.9459	4.1988	5.0090	6.0685	7.4425
	5	4.7355	5.1343	6.2228	8.0322	10.207
Case 3	1	2.9306	3.1082	3.7505	5.3653	10.124
	2	5.5469	5.7455	6.5128	8.4885	14.135
	3	7.0208	7.5606	9.4513	12.565	19.713
	4	9.5831	9.5315	10.220	14.084	25.735
	5	10.356	11.346	13.980	17.271	28.226
Case 4	1	3.6448	3.8679	4.6714	6.6575	12.534
	2	7.4373	7.3865	8.2692	10.826	18.344
	3	7.4374	8.3757	10.690	15.230	25.023
	4	10.965	11.109	12.119	16.128	32.022
	5	13.359	14.115	16.839	20.572	32.931
Case 5	1	2.2478	2.3661	2.7767	3.7149	6.0748
	2	2.6625	2.7558	3.0890	3.8948	6.1030
	3	4.3971	4.5282	5.0186	6.2744	9.8642
	4	6.2017	6.5377	7.4977	8.8512	12.075
	5	6.7936	7.1130	8.2153	10.603	15.716
Case 6	1	0.3518	0.3627	0.3984	0.4572	0.5395
	2	0.8624	0.8803	0.9541	1.1478	1.6442
	3	2.1578	2.2522	2.5636	2.7411	3.1791
	4	2.7559	2.6661	2.6253	3.2162	4.6977
	5	3.1382	3.4233	4.1867	5.1364	6.0521

However, the difference between two results is negligible except for plates with a high skew angle and with simple supports on all edge. To study the effect of relative thickness ratio (h/b), the frequency ratio (ω/ω_0) or (frequency)/(frequency obtained for thin plates when $h/b = 0.001$) is introduced in Table 10. The (ω/ω_0) values decrease with increasing thickness/span ratio and skew angle for CCCC edge condition (Case 4) when $v = 0.3$ and $a/b = 1.0$. This trend is most pronounced for the clamped case. In general, it may be concluded that the frequency parameter decreases as the thickness ratio h/b increases from 0.001 to 0.2 that can be confirmed in Tables 7 and 8. The decrease in the frequency parameter is due to the effects of shear deformation and rotatory inertia. These effects are more significant in the higher modes than in the lower modes.

Table 8
Frequency parameters $\lambda = (\omega b^2/\pi^2)\sqrt{\rho h/D}$ of skew thick plates with various edge conditions ($a/b = 1.0$, $v = 0.3$, $h/b = 0.2$)

Edge condition	Mode number	Skew Angle β				
		0°	15°	30°	45°	60°
Case 1	1	1.7637	1.8026	2.1239	2.8799	4.7456
	2	3.8497	3.7228	3.9967	4.7955	6.7707
	3	3.8497	4.2158	5.1391	6.5052	8.5327
	4	5.4989	5.4398	5.7002	6.9893	10.401
	5	6.5681	6.7836	7.5917	8.3615	11.025
Case 2	1	0.9096	0.9495	1.0853	1.3524	1.7129
	2	1.4257	1.3283	1.3794	1.4920	1.7992
	3	2.9393	2.7765	2.8038	2.9951	3.5119
	4	3.1676	3.2997	3.6761	3.9807	4.1052
	5	3.6296	3.6877	4.2027	5.0559	5.4778
Case 3	1	2.2615	2.3605	2.7336	3.5683	5.5062
	2	4.0354	4.0975	4.4573	5.3506	7.4286
	3	4.5145	4.7792	5.6505	7.0200	9.1025
	4	5.9272	5.8785	6.1650	7.4414	10.875
	5	6.6626	6.9815	7.9596	8.8146	11.344
Case 4	1	2.6875	2.7882	3.2217	4.1622	6.2381
	2	4.6908	4.6108	4.9621	5.9043	8.0706
	3	4.6908	5.0869	6.0136	7.4729	9.6438
	4	6.2986	6.2708	6.5790	7.8007	11.376
	5	7.1768	7.3881	8.2697	9.2237	11.543
Case 5	1	1.7765	1.8465	2.0788	2.5659	3.5597
	2	2.0016	2.0505	2.2205	2.6085	3.6353
	3	3.1113	3.2000	3.5000	4.1383	5.5005
	4	4.0401	4.1801	4.5983	5.2599	6.4559
	5	4.3200	4.4432	4.8697	5.8135	7.7400
Case 6	1	0.3383	0.3479	0.3768	0.4225	0.4791
	2	0.7432	0.7579	0.8146	0.9644	1.3415
	3	1.7797	1.8309	1.9752	2.1001	2.2427
	4	2.2712	2.1863	2.1606	2.3855	2.9414
	5	2.4097	2.6242	3.0925	3.6684	4.1418

From these results, it may be noted that the proposed *p*-version finite element model gives the reliable and accurate solutions regardless of the higher corner singularity due to the increase of obtuse angles and geometric constraints.

4.2. Skew plates with cutout

Published literature on vibration of skew plates with cutout is insufficient and rare, and an explicit solution for this problem is not established. In the present work, the skew Mindlin plate with a concentric cutout has been selected as a test problem with $h/b = 0.1$ and $v = 0.3$. The size of

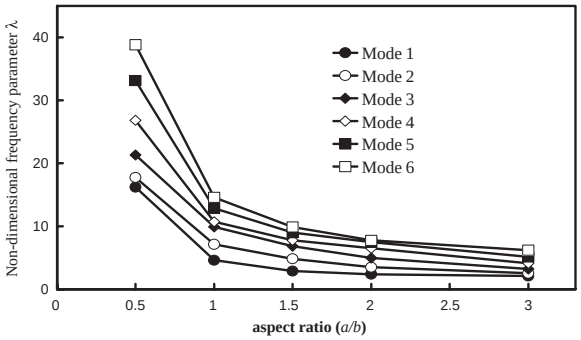

Fig. 7. Vibratory response to increase of aspect ratio a/b for skew plates with SCSC (Case 3) edge condition ($v=0.3$, $\beta=45^\circ$).

Table 9
Comparison of non-dimensional fundamental frequencies(λ_1) of thin skew plates with various edge conditions ($h/b=0.001$, $v=0.3$, $a/b=1.0$)

Edge condition	Fundamental frequencies for skew angles					
	0°	15°	30°	45°	60°	
Case 1	Raju [12]	2.0006	2.1172	2.5479	3.6664	7.0582
	Present	2.0000	2.1149	2.5380	3.5871	6.9160
Case 2	Liew [23]	0.9759	1.0334	1.2310	1.6649	2.5810
	Present	0.9759	1.0333	1.2314	1.6696	2.6195
Case 3	Raju [12]	2.9347	3.1122	3.7497	5.3300	9.8868
	Present	2.9306	3.1082	3.7505	5.3653	10.124
Case 4	Raju [12]	3.6481	3.8716	4.6744	6.6652	12.408
	Present	3.6448	3.8679	4.6714	6.6575	12.534
Case 5	Liew [23]	2.2462	2.3656	2.7763	3.6933	5.8584
	Present	2.2478	2.3661	2.7767	3.7149	6.0748
Case 6	Liew [23]	0.3517	0.3631	0.3983	0.4571	0.5346
	Present	0.3518	0.3627	0.3984	0.4572	0.5395

the cutout $a' \times b'$ are defined as $a'/a=0.25$, 0.5 and $b'/b=0.25$, 0.5. Four hierarchical elements shown in Fig. 8(a) are used to model it with p-level = 5, on the other hand, this skew plate with cutout is discretized by 256 four-noded elements by SAP2000 program that is also shown in Fig. 8(b). In case of SAP2000 model, the meshes are refined in the vicinity of obtuse corners due to moment singularity. Both finite element models are fixed from the convergence tests. Numerical results have been obtained for two different boundary conditions where the out edge and the inner edge are referred to as SSSS-FFFF (simply supported–free) and CCCC–FFFF (clamped–free). The non-dimensional frequency parameters for the six modes are plotted in Figs. 9 and 10 It may be noted that the non-dimensional frequency parameters become larger as the skew angle β is increased, especially beyond 45° for both cases. This trend is in line with case without cutout. The mode shapes are shown in Figs. 11 and 12 for the two stated edge conditions. For each skew angle, five mode shapes are shown. To verify the proposed element, the present solutions by four hierarchical elements have been compared with those obtained by SAP2000 program with respect

Table 10
Comparison of fundamental frequencies ratio(ω/ω_0) for thick skew plates with CCCC edge condition (Case 4, $v=0.3$, $a/b=1.0$)

h/b	Mode number	Fundamental frequencies ratio(ω/ω_0) for skew angles				
		0°	15°	30°	45°	60°°
0.1	1	0.9041	0.8866	0.8738	0.8397	0.7410
	2	0.8452	0.8357	0.8201	0.7812	0.6841
	3	0.8452	0.8280	0.7968	0.7271	0.6122
	4	0.8035	0.7918	0.7743	0.7297	0.5696
	5	0.7769	0.7626	0.7352	0.6815	0.5801
0.2	1	0.7373	0.7209	0.6897	0.6252	0.4977
	2	0.6307	0.6242	0.6001	0.5454	0.4400
	3	0.6307	0.6073	0.5626	0.4907	0.3854
	4	0.5744	0.5645	0.5429	0.4837	0.3553
	5	0.5372	0.5234	0.4911	0.4484	0.3505

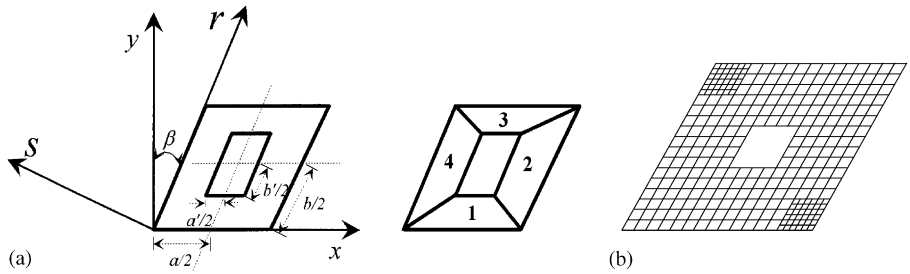

Fig. 8. Geometry and four-element *p*-version model for skew plates with cutout. (b) The 256-element *h*-version model by SAP2000 for skew plates with cutout.

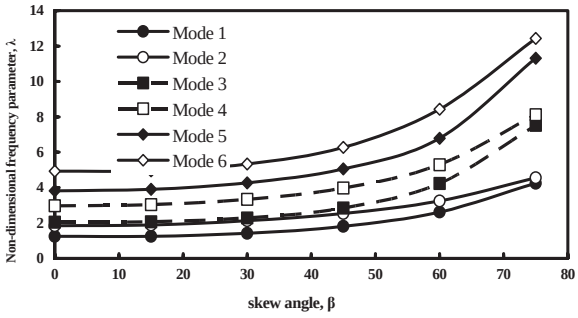

Fig. 9. Frequency parameters for SSSS–FFFF edge condition with respect to skew angle. ($a/b=a'/b'=2.0$, $a'/a=b'/b=0.5$, $h/b=0.1$, $v=0.3$).

to edge condition. In Figs. 13 and 14, it can be seen that the non-dimensional frequency parameters by *p*-version model agree very well with those by SAP2000 program for six modes.

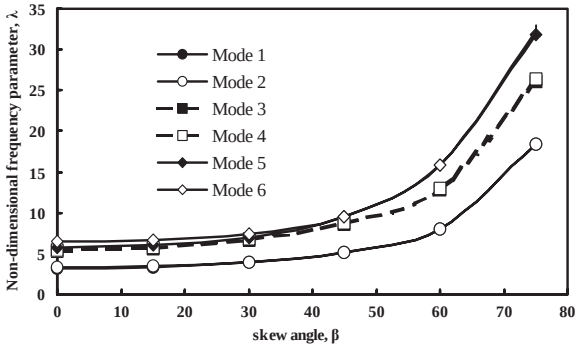

Fig. 10. Frequency parameters for CCCC–FFFF edge condition with respect to skew angle ($a/b = a'/b' = 2.0$, $a'/a = b'/b = 0.5$, $h/b = 0.1$, $v = 0.3$).

	Mode 1	Mode 2	Mode 3	Mode 4	Mode 5
Skew Angle 0	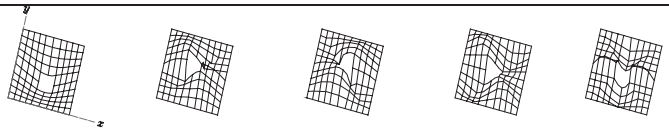				
λ	1.86648	4.13717	4.13717	6.68906	8.07507
Skew Angle 45	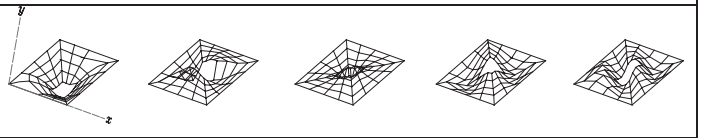				
λ	2.89810	5.49548	6.13382	8.51635	11.19775

Fig. 11. The mode shapes of skew plates with cutout for SSSS–FFFF edge condition. ($a/b = a'/b' = 1.0$, $a'/a = b'/b = 0.25$, $h/b = 0.1$, $\nu = 0.3$).

	Mode 1	Mode 2	Mode 3	Mode 4	Mode 5
Skew Angle 0	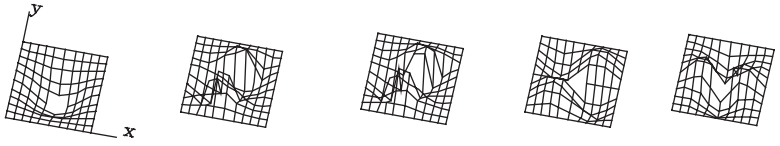				
λ	3.47917	5.54329	5.54329	8.01027	9.5268
Skew Angle 45	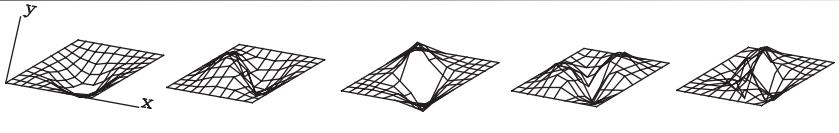				
λ	5.72467	8.00692	8.02873	10.91378	13.34978

Fig. 12. The mode shapes of skew plates with cutout for CCCC–FFFF edge condition. ($a/b = a'/b' = 1.0$, $a'/a = b'/b = 0.25$, $h/b = 0.1$, $\nu = 0.3$).

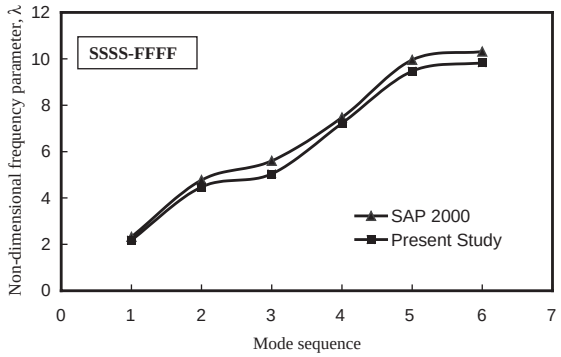

Fig. 13. Comparison of non-dimensional frequencies of skew plates with cutout for SSSS–FFFF edge condition. ($a/b = a'/b' = 1.0$, $a'/a = b'/b = 0.25$, $h/b = 0.1$, $v = 0.3$, $\beta = 30^\circ$).

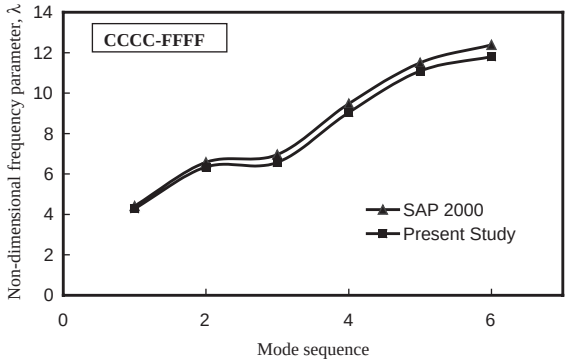

Fig. 14. Comparison of non-dimensional frequencies of skew plates with cutout for CCCC–FFFF edge condition. ($a/b = a'/b' = 1.0$, $a'/a = b'/b = = 0.25$, $h/b = 0.1$, $v = 0.3$, $\beta = 30^\circ$).

Also the values of λ are tabulated in Tables 11 and 12. In these tables, the first six frequency parameters are presented for two aspect ratios ($a/b = 1.0$ and 2.0), three skew angles ($\beta = 0^\circ$, 30°, and 60°), and two thickness–width ratios ($h/b = 0.001$ and 0.1). It is noted that the frequency parameters decrease as a/b ratio is increased from 1 to 2, and the plate becomes thicker. On the other hand, a higher frequency response has been observed as the skew angle is increased, and the edge constraints are more pronounced from SSSS–FFFF to CCCC–FFFF edge condition. These results are very similar to the case without cutout.

5. Conclusions

Free vibration analysis of skew plates based on Mindlin theory based on *p*-version finite element formulation and Houserholder QR iteration method was successfully implemented. Numerical results were obtained for two different types of plate with/without cutout. Different

Table 11
Non-dimensional frequency parameters, $\lambda = (\omega b^2/\pi^2)\sqrt{\rho h/D}$, of skew plates with cutout for SSSS–FFFF edge condition ($v = 0.3$)

a/b	a'/a and b'/b	β (deg)	h/b	Mode sequence number					
				1	2	3	4	5	6
		0	0.001	1.9473	4.7048	4.7048	7.6195	9.6224	11.146
			0.1	1.8665	4.1372	4.1372	6.6891	8.0751	9.4864
		30	0.001	2.4400	5.1540	6.3896	8.4695	11.831	12.249
	0.25		0.1	2.1855	4.4755	5.0336	7.2215	9.4625	9.8338
		60	0.001	6.3059	10.116	14.658	15.582	20.912	26.354
1.0			0.1	4.5885	7.8816	8.1019	11.684	14.653	15.147
		0	0.001	2.3791	4.1229	4.1229	7.2368	7.6755	11.472
			0.1	2.2390	3.5357	3.5357	5.8642	6.3300	9.1526
		30	0.001	2.9169	4.7444	4.9411	8.3797	8.7395	12.228
	0.5		0.1	2.4579	3.6488	4.0892	6.3138	6.9907	9.6694
		60	0.001	7.1301	9.5353	9.8689	14.915	16.138	21.165
			0.1	4.4184	5.2624	6.9272	8.5279	11.255	13.785
		0	0.001	1.1582	1.9634	3.3804	3.5094	4.7966	4.9781
			0.1	1.1178	1.8624	2.9601	3.1142	4.3703	4.3806
		30	0.001	1.4586	2.4014	3.8370	4.2525	5.8093	6.2042
	0.25		0.1	1.3562	2.2242	3.3842	3.5090	4.7831	5.3889
		60	0.001	3.4789	5.5958	8.1517	8.5565	10.392	14.462
			0.1	2.9456	4.6631	5.2409	6.3613	7.9206	9.5680
2.0		0	0.001	1.3114	1.9878	2.4254	3.4824	4.2606	5.6052
			0.1	1.2518	1.8474	2.0495	2.9679	3.8197	4.9375
		30	0.001	1.6103	2.4232	2.7656	4.0023	4.9754	6.2150
	0.5		0.1	1.4284	2.1302	2.2881	3.3348	4.2750	5.3272
		60	0.001	3.6128	4.8268	5.5104	7.8953	8.8542	11.222
			0.1	2.6189	3.2487	4.2327	5.2985	6.7937	8.4339

combinations of boundary conditions, aspect ratios, skew angles and thickness/span ratios were considered.

The study shows that the effects of shear deformation and rotatory inertia effect on the frequency parameters are more significant for skew plates with relatively high values of thickness–width ratios and skew angles. Also, it is noted that the frequency parameters decrease as a/b ratio is increased, and the plate becomes thicker. On the other hand, a higher frequency response has been observed as the skew angle is increased, and the edge constraints are more pronounced from simply supported to clamped edges. As expected, convergence of frequency is monotonic from above results as the p-level is increased from 1 to 13.

The p-version model presented herein offers a reliable tool for vibration analysis of skew plates, as demonstrated by the numerous parametric studies. From the point of view of versatility, accuracy, and economy of solution, it can be concluded that the p-version of the finite element method is highly robust and appropriate technique for solving eigenvalue problems of the continua.

Table 12
Non-dimensional frequency parameters, $\lambda = (\omega b^2/\pi^2)\sqrt{\rho h/D}$, of skew plates with cutout for CCCC–FFFF edge condition (ν=0.3)

A/b	a'/a and b'/b	β (deg)	h/b	Mode sequence number					
				1	2	3	4	5	6
		0	0.001	3.8805	6.9137	6.9137	10.356	12.783	15.581
			0.1	3.4792	5.5433	5.5433	8.0103	9.5268	11.557
		30	0.001	4.9298	7.9785	8.9953	11.986	15.763	16.759
	0.25		0.1	4.2787	6.3521	6.5743	9.0462	11.095	11.805
		60	0.001	12.688	17.508	19.654	24.320	31.772	35.736
1.0			0.1	9.3978	11.365	12.071	15.434	17.316	17.992
		0	0.001	6.6233	7.7764	7.7764	10.705	10.969	15.233
			0.1	5.6601	6.2750	6.2750	7.7619	8.2804	10.704
		30	0.001	8.5601	9.6002	9.9690	12.894	13.022	16.947
	0.5		0.1	7.0668	7.4756	7.8024	9.0083	9.6784	11.968
		60	0.001	9.6018	10.346	13.256	14.849	16.000	21.997
			0.1	7.4117	7.5555	9.4040	9.4949	10.703	12.111
		0	0.001	2.6290	3.1886	4.8839	5.2460	6.5701	6.8623
			0.1	2.4167	2.7881	4.1397	4.1757	5.4008	5.5741
		30	0.001	3.4174	4.0129	5.8095	6.4229	7.9217	8.8652
	0.25		0.1	3.0614	3.4115	4.8604	4.8828	6.0904	6.7960
		60	0.001	9.6018	10.346	13.256	14.849	16.000	21.997
			0.1	7.4117	7.5555	9.4040	9.4949	10.703	12.111
	0.5		0.001	3.7572	3.7763	6.2590	6.7325	6.9902	8.2057
			0.1	3.2065	3.2681	5.3016	5.4852	5.7610	6.4769
			0.001	4.7452	4.7642	7.9853	8.3352	8.7045	9.6321
			0.1	3.8965	3.9653	6.6127	6.7177	6.9114	7.4280
			0.001	11.936	11.989	19.113	19.351	23.638	23.680
			0.1	7.9611	8.0125	12.790	12.915	15.814	15.908

References

[1] L.S.D. Morley, Bending of simply supported rhombic plates under uniform normal loading, Quarterly Journal of Mechanics and Applied Mathematics 15 (1962) 414–426.

[2] A.W. Leissa, Recent research in plate vibration: classical theory, The Shock and Vibration Digest 9 (10) (1977) 13–24.

[3] A.W. Leissa, Recent studies in plate vibration: 1981–1985, Part I: classical theory, The Shock and Vibration Digest Digest 19 (2) (1987) 11–18.

[4] H.D. Conway, K.A. Farnham, The free flexural vibrations of triangular, rhombic and parallelogram plates and some analogies, International Journal of Mechanical Sciences 7 (1965) 811–816.

[5] P.S. Nair, S. Durvasula, Vibration of skew plates, Journal of Sound and Vibration 26 (1973) 1–19.

[6] I.H. Tai, W.A. Nash, Vibrations of thin plates—a new approach, Department of Civil Engineering, University of Massachusetts, Report No. AFOSR-TR-0789, (1973).

[7] I. Chopra, S. Durvasula, Natural frequencies and modes of tapered skew plates, International Journal of Mechanical Sciences 13 (1971) 935–944.

[8] T. Sakata, Natural frequencies of simply supported skew plates, International Journal of Mechanical Sciences 23 (1981) 677–685.

[9] K. Nagaya, Vibration of a plate with straight line boundaries, Journal of Sound and Vibration 68 (1) (1980) 35–43.
[10] D.J. Gorman, Accurate analytical type solutions for the free vibration of simply supported parallelogram plates, American Society of Mechanical Engineers Journal of Applied Mechanics 58 (1) (1991) 203–208.
[11] N.N. Rao, S. Durvasula, M.V. Rao, R. Samuel, Vibration of simply supported skew plates—an experimental study, Proceedings of the 19th Midwest Mechanics Conference, 1985. (2 page extended abstract).
[12] K.K. Raju, E. Hinton, Natural frequencies and modes of rhombic Mindlin plates, Earthquake Engineering and Structural Dynamics 8 (1980) 55–62.
[13] O.G. McGee, A.W. Leissa, Three-dimensional free vibrations of thick skewed cantilevered plates, Journal of Sound and Vibration 144 (2) (1991) 305–322.
[14] O.G. McGee, A.W. Leissa, S. Huang, Vibrations of cantilevered skewed plates with corner stress singularities, International Journal for Numerical Methods in Engineering 35 (1992) 409–424.
[15] N.S. Bardell, Free vibration analysis of a flat plate using the hierarchical finite element method, Journal of Sound and Vibration 151 (2) (1991) 263–289.
[16] O. Beslin, J. Nicolas, Ahierarchical functions set for predicting very high order plate bending modes with any boundary conditions, Journal of Sound and Vibration 202 (5) (1997) 633–655.
[17] P. K. Basu, M. P. Rossow, B. A. Szabo, Theoretical Manual and Users Guide for COMET-X, Report FRA/ORD-77/60, Washington University, 1977.
[18] C.S. Huang, O.G. McGee, A.W. Leissa, J.W. Kim, Accurate vibration analysis of simply supported rhombic plates by considering stress singularities, Journal of Vibration and Acoustics 117 (1995) 245–251.
[19] T.S. Butalia, T. Kant, V.D. Dixit, Performance of heterosis element for bending of skew rhombic plates, International Journal of Computers and Structures 34 (1) (1990) 23–49.
[20] K.M. Liew, Y. Xiang, S. Kitipornchai, Transverse vibration of thick rectangular plates—I. Comprehensive sets of boundary conditions, International Journal of Computers and Structures 49 (1) (1993) 1–29.
[21] K.M. Liew, Y. Xiang, S. Kitipornchai, Transverse vibration of thick rectangular plates—II Inclusion of oblique internal line supports, International Journal of Computers and Structures 49 (1) (1993) 31–58.
[22] K.M. Liew, Y. Xiang, S. Kitipornchai, Transverse vibration of thick rectangular plates—III Effects of multiple eccentric internal ring supports, International Journal of Computers and Structures 49 (1) (1993) 59–67.
[23] K.M. Liew, Y. Xiang, S. Kitipornchai, C.M. Wang, Vibration of thick skew plates based on Mindlin shear deformation plate theory, Journal of Sound and Vibration 168 (1) (1993) 39–69.